

## Catalysts Transform While Molecules React: An Atomic-Scale View

Zhenxing Feng,<sup>†,‡</sup> Junling Lu,<sup>§</sup> Hao Feng,<sup>§</sup> Peter C. Stair,<sup>†</sup> Jeffrey W. Elam,<sup>§</sup> and Michael J. Bedzyk<sup>\*,†,‡</sup>

<sup>†</sup>Department of Materials Science and Engineering, <sup>‡</sup>Department of Chemistry, and <sup>#</sup>Department of Physics and Astronomy, Northwestern University, Evanston, Illinois 60208, United States

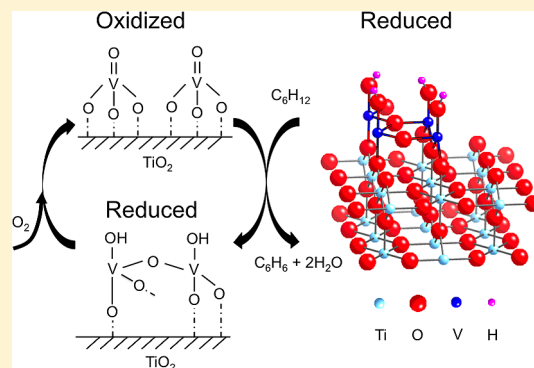
<sup>‡</sup>Electrochemical Energy Laboratory, Massachusetts Institute of Technology, Cambridge, Massachusetts 02139, United States

<sup>§</sup>Energy Systems Division, Argonne National Laboratory, Argonne, Illinois 60439, United States

### Supporting Information

**ABSTRACT:** We explore how the atomic-scale structural and chemical properties of an oxide-supported monolayer (ML) catalyst are related to catalytic behavior. This case study is for vanadium oxide deposited on a rutile  $\alpha$ -TiO<sub>2</sub>(110) single-crystal surface by atomic layer deposition (ALD) undergoing a redox reaction cycle in the oxidative dehydrogenation (ODH) of cyclohexane. For measurements that require a greater effective surface area, we include a comparative set of ALD-processed rutile powder samples. In situ single-crystal X-ray standing wave (XSW) analysis shows a reversible vanadium oxide structural change through the redox cycle. Ex situ X-ray photoelectron spectroscopy (XPS) shows that V cations are 5+ in the oxidized state and primarily 4+ in the reduced state for both the (110) single-crystal surface and the multifaceted surfaces of the powder sample. In situ diffuse reflectance infrared Fourier transform spectroscopy, which could only achieve a measurable signal level from the powder sample, indicates that these structural and chemical state changes are associated with the change of the V=O vanadyl group. Catalytic tests on the powder-supported VO<sub>x</sub> revealed benzene as the major product. This study not only provides atomic-scale models for cyclohexane molecules interacting with V sites on the rutile surface but also demonstrates a general strategy for linking the processing, structure, properties, and performance of oxide-supported catalysts.

**SECTION:** Surfaces, Interfaces, Porous Materials, and Catalysis



Heterogeneous catalysts are crucial for industrial and environmental applications such as petroleum refining<sup>1</sup> and the selective catalytic reduction of automotive and industrial NO<sub>x</sub> emissions.<sup>2</sup> A fundamental understanding of the interactions between chemical species and catalytically active surfaces is vital for advancing the science of heterogeneous catalysis and developing industrial applications. Supported vanadium oxide (VO<sub>x</sub>) is an important and commonly used model catalytic system due to its rich and diverse chemistry.<sup>3</sup> Much work has focused on the atomic-scale structural properties of VO<sub>x</sub> during chemical reactions.<sup>3–7</sup> Furthermore, supported VO<sub>x</sub> has also been intensively investigated for the oxidative dehydrogenation (ODH) of ethanol, propane, and cyclohexane due to its high catalytic reactivity and selectivity.<sup>8–11</sup> During a catalytic turnover, the vanadium cation undergoes reduction and reoxidation. However, the atomic-scale structural and oxidation state changes in the catalytic VO<sub>x</sub> surface species that are associated with the catalytic cycle are poorly understood at best. Although the structure of oxidized VO<sub>x</sub> is believed to have a four-coordinate distorted tetrahedral geometry with a vanadium–oxygen double bond,<sup>12</sup> the atomic-scale structure can be complicated under different conditions such as different V coverages and supports.<sup>3,4,6,13,14</sup> The structure of the reduced

species is essentially unknown. This absence of detailed structural information makes it difficult to establish the relationships between the atomic structure, composition, electronic properties, and catalytic performance.<sup>15</sup>

Spectroscopic and structural studies of oxidation catalysts under reaction conditions only provide information on the most abundant surface species, typically in the oxidized state. However, when the catalytic cycle can be broken up into two half-cycles corresponding to reduction and reoxidation, it is possible to trap the catalyst in its reduced state and perform detailed structure and spectroscopic measurements. This strategy is employed in the present study.

Recently, we reported the surface structural changes of monolayer<sup>4</sup> (ML) and sub-ML<sup>13</sup> VO<sub>x</sub> supported on rutile  $\alpha$ -TiO<sub>2</sub>(110) during reduction–oxidation (redox) reactions using H<sub>2</sub> and O<sub>2</sub> gas. Our findings showed that different V coverages led to different V structural and chemical state changes. In this present study, to better understand these structure–activity relationships, the molecular structure of VO<sub>x</sub> species on both rutile TiO<sub>2</sub>(110) single-crystal surfaces and

**Received:** November 14, 2012

**Accepted:** December 26, 2012

powders are explored under oxygen oxidative and cyclohexane reducing environments by combining in situ X-ray standing waves (XSW), in situ diffuse reflectance infrared Fourier transform spectroscopy (DRIFTS), and ex situ X-ray photoelectron spectroscopy (XPS). V atomic structural maps from the XSW measurements are recorded for the oxidized (Ox), reduced (Re), and reoxidized (Ox2) interfaces. The XSW-observed structural changes are associated with changes in both the chemical state and bonding of the interfacial V, as observed by XPS and DRIFTS, respectively. Next, selectivity and reactivity tests are performed. The structural and chemical information provided by XSW, XPS, and DRIFTS are linked to catalytic performance, demonstrating a general strategy for understanding the structure–property relationship at the atomic scale.

Polished  $\alpha$ -TiO<sub>2</sub>(110) single-crystal substrates were cleaned and oxygen-annealed to obtain atomically flat surfaces. ( $\alpha$  refers to the rutile phase of TiO<sub>2</sub>.) The substrates were then exposed to two atomic layer deposition (ALD) growth cycles to grow 1.5 ML VO<sub>x</sub>. One ML is defined as the area density of Ti atoms in the TiO(110) plane, or 10.4 atoms/nm<sup>2</sup>. These samples are denoted as 2c-s, where “c” stands for the ALD cycle and “s” stands for single crystal. Atomically flat terraces were observed by atomic force microscopy (AFM) before and after the ALD (see Figure S1 in the Supporting Information (SI)), indicating a conformal film-like structure on the surface. VO<sub>x</sub> was also deposited on rutile powders. The ALD precursor exposure and purge times were increased to account for the larger surface area and increased vapor transport time for the powder relative to coating planar surfaces. Three and six ALD cycles of VO<sub>x</sub> were deposited, denoted as 3c-p and 6c-p, where “p” stands for powder.

Ex situ XPS was used to examine the chemical states of the surface atoms supported on both single crystals and powders after each step of the reaction process, namely, the as-deposited (AD), Ox, Re, and Ox2 conditions. Figure 1a shows the XPS spectra of the 2c-s sample at the Ox and Re states.<sup>16</sup> XPS of

Ox2 (not shown) was virtually identical to the XPS of Ox, indicating reversibility of the VO<sub>x</sub> chemical states. We used data processing and assignment methods described elsewhere for fitting the XPS peaks.<sup>5,17,18</sup> As seen in Figure 1a for the Ox state, the V 2p<sub>3/2</sub> binding energy (BE) is 517.2 eV, and the binding energy difference (BED) between the O 1s and V 2p<sub>3/2</sub> is 12.8 eV. This indicates that V is V<sup>5+</sup> for the Ox state. However, in the Re state, the V 2p<sub>3/2</sub> peak became broader, indicating the coexistence of multiple chemical states. Detailed analysis shows that these V's were composed of 61% V<sup>4+</sup> (BED: 14.0 eV) and 39% V<sup>5+</sup>. This 61% transformation of V<sup>5+</sup> → V<sup>4+</sup> after cyclohexane reduction is similar to that of our previous study of 2 ML VO<sub>x</sub>/α-TiO<sub>2</sub>(110), for which H<sub>2</sub> was used as the reductant and where we saw 100% transformation.<sup>4</sup> It is not surprising to observe this partial reduction of V<sup>5+</sup> to V<sup>4+</sup> in an ambient condition because of the coexistence of multiple chemical states of V. This has similarly been reported for V on silica, alumina, and zirconia,<sup>19,20</sup> which, like titania, are also difficult to reduce.

In situ XSW analysis<sup>21–23</sup> was used to measure the V atomic density map relative to the rutile substrate lattice. XSW combines single-crystal X-ray diffraction with X-ray fluorescence (XRF). Unlike conventional diffraction methods, the XSW method is element-specific (via XRF) and does not suffer from the so-called “phase problem”. Therefore, it is straightforward to produce a model-independent 3D map,  $\rho(\mathbf{r})$ , for the XRF-selected atomic species by the summation<sup>24–27</sup>

$$\rho(\mathbf{r}) = 1 + \sum_{\mathbf{H} \neq -\mathbf{H}, \mathbf{H} \neq 0} f_{\mathbf{H}} \cos[2\pi(\mathbf{P}_{\mathbf{H}} - \mathbf{H} \cdot \mathbf{r})] \quad (1)$$

which uses the XSW-measured Fourier amplitudes  $f_{\mathbf{H}}$  and phases  $P_{\mathbf{H}}$  from each  $\mathbf{H} = hkl$  substrate reflection examined. Figure 1b shows the XSW data and fit for the TiO<sub>2</sub>(110) Bragg peak. The V K $\beta$  fluorescence yield was analyzed for each redox processing step.<sup>28</sup> The different shapes of these yields in the Ox and Re states indicate that there are different V structures under these two different conditions. An extremely low value for the 110 Fourier amplitude,  $f_{110} = 0.07$ , was found for the Ox condition, indicating that V atoms are uncorrelated with the substrate lattice. This was also found in our previous study of the Ox 2 ML VO<sub>x</sub>/α-TiO<sub>2</sub>(110)<sup>4</sup> but not for our recent sub-ML case.<sup>13</sup> In the Re state, the very asymmetric V K $\beta$  yield (Figure 1b) gives a relatively high Fourier amplitude,  $f_{110} = 0.61$ , indicating that the surface V cations are highly correlated with the substrate lattice in a direction normal to the 110 planes. Therefore, more XSW measurements (Figure S3, SI) in the Re state were made for other  $hkl$  diffraction planes. The results are shown in Table 1. Interestingly, the Fourier amplitudes for all of these measured planes had high values,

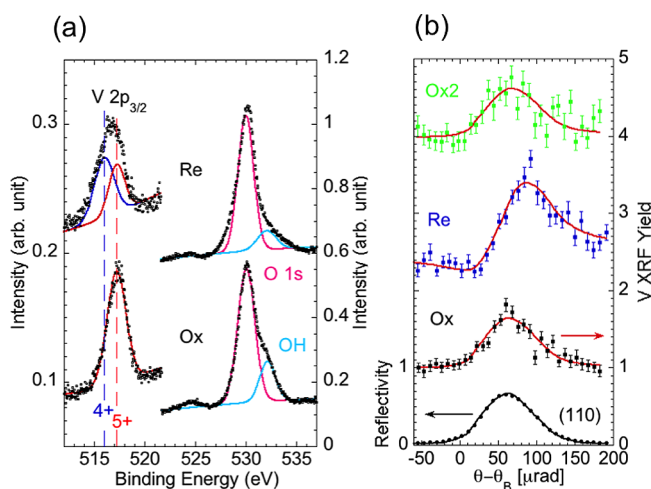


**Figure 1.** (a) Ex situ X-ray photoelectron spectra and (b) in situ (110) XSW analysis for the same 1.5 ML VO<sub>x</sub>/α-TiO<sub>2</sub>(110) surface after the O<sub>2</sub> oxidation (Ox) and cyclohexane reduction (Re) processing steps. (a) V changes from 100% V<sup>5+</sup> for the Ox to a mixture of 61% V<sup>4+</sup>–39% V<sup>5+</sup> for the Re surface. (b) The V atomic distribution changes from uncorrelated (Ox) to 60% correlated (Re) and reversibly back to uncorrelated (Ox2).

**Table 1.** Summary of the XSW Experimental Results (meas) and Model-Dependent Fitting Results (calc) from the Re Surface of the 1.5 ML VO<sub>x</sub>/α-TiO<sub>2</sub> (110)<sup>a</sup>

$hkl$	$f_{\text{meas}}$	$f_{\text{calc}}$	$P_{\text{meas}}$	$P_{\text{calc}}$
110	0.61(3)	0.60	0.02(1)	0.04
101	0.65(6)	0.60	−0.05(2)	0.02
200	0.50(9)	0.60	−0.03(4)	0.04
211	0.60(9)	0.60	0.03(4)	0.06

<sup>a</sup> $f$  and  $P$  are the Fourier amplitude and phase, respectively, for the V atomic distribution.

indicating a strong 3D correlation for the V atom distribution relative to the substrate lattice in the Re state. For the Ox2 state,  $f_{110} = 0.12$  is a reasonably good match for  $f_{110} = 0.07$  in the Ox state. This structural information is consistent with the reversibility of  $\text{VO}_x$  during the redox reaction, as observed chemically by the XPS results. These findings are consistent with our earlier study.<sup>4</sup> In both cases, redox causes V cations to undergo a reversible correlated–uncorrelated transformation concurrent with an XPS-observed oxidation state transformation from  $\text{V}^{4+}$  to  $\text{V}^{5+}$ , respectively.

By inserting all XSW-measured Fourier components (and their symmetry equivalents) into eq 1, a V atomic density map was created, as shown in Figure 2. This density map is

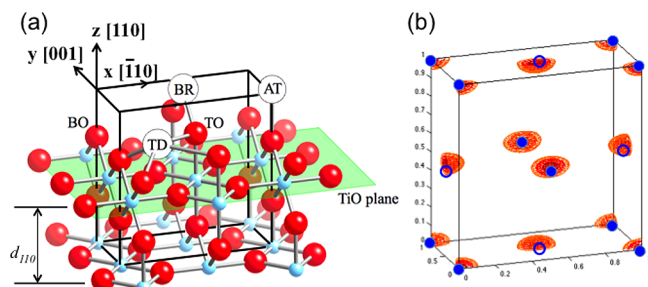


**Figure 2.** XSW-measured 3D vanadium atomic density map for ALD-grown 1.5 ML  $\text{VO}_x/\alpha\text{-TiO}_2(110)$  after the surface was reduced by cyclohexane. (a) A  $\text{TiO}_2(110)$  ball-and-stick model with O atoms in red and Ti in light blue. The nonprimitive unit cell for the (110) surface (outlined in black) has a height of  $2d_{110} = 6.50 \text{ \AA}$ . The model shows a possible surface termination that has both bridging (BO) and terminal (TO) oxygen atoms. Possible cation adsorption sites include atop (AT), bridging (BR), and tetradentate (TD). (b) V atomic density map superimposed on same unit cell as that in (a) with the AT and BR symmetry-inequivalent Ti sites shown as solid and open circles, respectively. The V density maxima are laterally aligned with sites AT and BR but shifted slightly upward.

superimposed onto the substrate  $\text{TiO}_2$  unit cell, which is outlined in black in Figure 2a. Figure 2a also shows adsorption sites, in which the atop (AT or A) and bridge (BR or B) sites are the two symmetry-inequivalent bulk-like Ti sites.<sup>29,30</sup> Analysis (Figure S4 and Table S1, SI) of the 3D map (Figure 2) shows that V atoms equally occupy these two sites and that the spatial positions of the density maxima for both are displaced  $0.05 \text{ \AA}$  slightly higher than the ideal Ti bulk-like positions. This XSW finding, together with the XPS finding of  $\text{V}^{4+}$  for the Re surface, is consistent with the formation of a rutile  $\text{VO}_2$  structure having pseudo-morphic epitaxy with the underlying rutile  $\text{TiO}_2$  crystal. This is not surprising because bulk  $\text{VO}_2$  has a rutile crystal structure, and the formation of highly coherent  $\text{VO}_2$  films isostructural to the  $\text{TiO}_2$  rutile substrate have been reported for various growth methods.<sup>14,31–33</sup> Ti K XRF signals from the bulk  $\text{TiO}_2$  were also analyzed (Figure S5 and Table S2, SI) to ensure the validity of the XSW analysis.

To better quantify the V surface site geometry for the Re case, a model is used based on the rutile-on-rutile structure described above. Because the Fourier amplitudes for each of the measured  $hkl$  reflections was roughly 0.6, we would conclude that 0.9 ML of the 1.5 ML V are correlated  $\text{V}^{4+}$  in the Re state. Therefore, a single layer, instead of two rutile-like pseudo-morphic layers,<sup>4</sup> is used as the model. In this model, V ions take Ti sites, X (=AT or BR), with occupation fractions,  $c_X$ , and

heights,  $h_X$ , above the  $\text{TiO}$  plane. The fitting results show that the two sites are occupied equally ( $c_A = c_B$ ) with the total occupation fraction,  $c_A + c_B = 0.60$ , indicating that 60% of the V ions are correlated to the substrate lattice. Model-dependent fitting also shows that the V heights are at  $3.32 \text{ \AA}$  above the  $\text{TiO}$  plane for both sites. This is  $0.07 \text{ \AA}$  higher than the ideal Ti site. For the Re surface, it is very interesting to note that the fraction (0.60) of V found by XPS in the  $\text{V}^{4+}$  chemical state matches the XSW-measured V correlated fraction.

To further understand how V ions undergo the correlated–uncorrelated transformation and how this structural change relates to interactions with cyclohexane and catalytic behavior, in situ DRIFTS and catalytic tests were carried out. Due to the limited surface area of the single-crystal-supported V, powder-supported V samples were used for both measurements. To ensure that the powder-supported V behaved catalytically the same as the single-crystal-supported V, XPS was performed. These measurements revealed that both the single-crystal and powder-supported ML V undergo the same redox cycle, that is, oxidized by  $\text{O}_2$  and reduced by cyclohexane under the same reaction conditions. Ex situ XPS measurements for both sets of samples (Figures 1a and S6, SI) showed the same trend for the electronic structural changes, namely,  $\text{V}^{5+}$  was found in the Ox state, while  $\text{V}^{4+}$  for ML V was found in the Re state. This strongly argues that the catalytic behavior of the  $\text{VO}_x$  should be the same on both the powders and the rutile (110) single-crystal surfaces. Consequently, results obtained from the cyclohexane ODH tests on the powder can be correlated to the  $\text{VO}_x$  structural changes measured on the single crystal.

The vibrational features from  $\text{VO}_x$  species (on  $\text{TiO}_2$ ) are usually obscured in the IR region due to the strong skeletal absorption of  $\text{TiO}_2$  below  $1000 \text{ cm}^{-1}$ .<sup>34–37</sup> To measure the spectral features contributed from surface  $\text{VO}_x$  species, the background for the DRIFTS measurements was taken on the dry pure rutile powder and subtracted from the  $\text{VO}_x/\text{TiO}_2$  spectra. Figure 3 shows the in situ background-subtracted DRIFTS measurements on  $\text{VO}_x$  (six ALD cycles) supported on

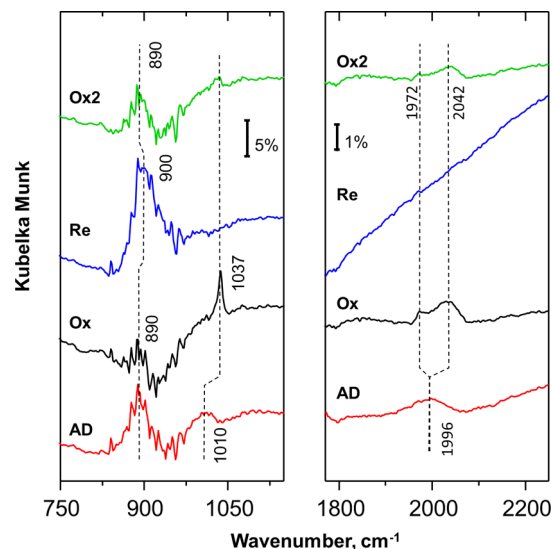


**Figure 3.** In situ DRIFTS measurements of  $\text{VO}_x$  supported on rutile  $\text{TiO}_2$  powder after sequential oxidation and reduction using  $\text{O}_2$  and cyclohexane, respectively. The wavenumber regions, shown on the left- and right-hand sides, are from the same individual infrared spectra collected after each treatment step.

rutile powder. Changes in the V bonding configuration are clearly seen when comparing the spectra for the AD, Ox, Re, and Ox2 surfaces. For the AD sample, the weak peak at 1010  $\text{cm}^{-1}$  is assigned to hydrated V=O double bonds in monomeric  $\text{VO}_x$  species.<sup>38–41</sup> The peak at 890  $\text{cm}^{-1}$  is assigned to the V–O–V stretching mode in the polymeric  $\text{VO}_x$  species.<sup>39,41</sup> To the best of our knowledge, this is the first reported observation of the V–O–V stretching mode using DRIFTS on  $\text{TiO}_2$ -supported  $\text{VO}_x$  catalysts. As discussed elsewhere, the broad band at 1996  $\text{cm}^{-1}$  is the first overtone of the fundamental V=O stretch, observed at 1010  $\text{cm}^{-1}$ .<sup>34,37</sup> After the first oxidation, the peak for the V=O bond becomes more pronounced and is shifted higher in wavenumber to 1037  $\text{cm}^{-1}$  as a consequence of dehydration.<sup>34,38,40</sup> Meanwhile, the decrease of the peak at  $\sim 890$   $\text{cm}^{-1}$  from AD to Ox is the result of the breakdown of polymeric  $\text{VO}_x$  species after oxidation. The first overtone splits into two bands at 2042 and 1972  $\text{cm}^{-1}$ , which are assigned to the overtone of dehydrated monomeric and polymeric  $\text{VO}_x$  species, respectively.<sup>34–37</sup> This is consistent with the XSW finding of uncorrelated  $\text{VO}_x$  in Ox. The V=O feature is also evidence for  $\text{V}^{5+}$ . Cyclohexane reduction (Re in Figure 3) causes the V=O stretch band to disappear along with its first overtone, indicating a dramatic change in the  $\text{VO}_x$  structure and chemical state. The increase of the V–O–V absorbance peak and simultaneous blue shift to 900  $\text{cm}^{-1}$  suggest an aggregation of polymeric  $\text{VO}_x$  species.<sup>39,41</sup> This is also consistent with the above-described XSW findings, which indicate the formation of a correlated  $\text{VO}_2$  rutile structure pseudo-morphic to the underlying rutile substrate. After the second oxidation (Ox2 in Figure 3), there is a similarity with the Ox spectrum that indicates the reversibility in agreement with the XSW and XPS measurements. The less pronounced V=O stretch at 1037  $\text{cm}^{-1}$  compared with the one in the Ox spectrum, may be due to an incomplete structural reversibility. Most importantly, the peak in the 850–950  $\text{cm}^{-1}$  region decreases. The similarity in this region for Ox and Ox2 shows that V–O–V linkages are weakened by oxidization for  $\text{VO}_x$  on  $\text{TiO}_2$  surfaces, resulting in the uncorrelated  $\text{VO}_x$  structure observed by XSW. The observation of vanadyl bond reduction by a cyclohexane molecule in our studies is consistent with that in previous studies,<sup>42,43</sup> which have shown that the reactivity of  $\text{VO}_x$  catalysts in the ODH reactions is closely correlated with the reducibility of the vanadyl group. However, the present work demonstrates that significant structural changes, including movement of vanadium atoms, accompany the reduction from 5+ to 4+. The reduction cannot be simply described as a loss of vanadyl oxygen.

Catalytic tests were carried out on powder-supported  $\text{VO}_x$ . These tests revealed that during cyclohexane ODH, benzene was the major reaction product, and the selectivity to cyclohexene was low (<5%) in the temperature range of 325–425 °C (See Figures S8 and S9, SI). The selectivity to benzene and cyclohexane both gradually decreased, while the selectivity to  $\text{CO}_2$  and CO apparently increased at above 350 °C.

On the basis of information obtained from XSW, XPS, DRIFTS, and the catalytic tests, we propose the model depicted in Figure 4a to explain the process of cyclohexane ODH on  $\alpha$ - $\text{TiO}_2(110)$ -supported ML  $\text{VO}_x$ . This model shows how cyclohexane molecules transform the surface  $\text{VO}_x$ . After oxidization,  $\text{VO}_x$  forms tetrahedral  $\text{VO}_4$  species with  $\text{V}^{5+}$  terminated by V=O bonds and bonded to three oxygen atoms below. Stereochemically, the symmetry of these

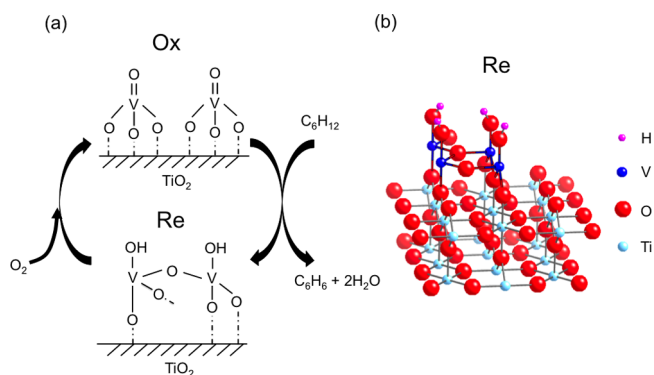


**Figure 4.** Model for cyclohexane ODH to benzene on ML V supported by rutile. (a) Cartoon models show the geometrical and chemical bonding changes of ML V in reaction. For the Ox surface, the  $\text{V}^{5+}$  with a tetrahedral  $\text{VO}_4$  structure is weakly bonded to the  $\text{TiO}_2$  surface, while in the Re state, a  $\text{VO}_2$  rutile-like structure is formed. (b) XSW-based atomic-scale interface model for a Re state showing  $\text{V}^{4+}$  cations equally occupying the two symmetry-inequivalent Ti sites (atop and bridge sites) on the  $\alpha$ - $\text{TiO}_2(110)$  surface.

tetrahedra does not match the two-fold symmetry of the  $\text{TiO}_2(110)$  rectangular surface unit cell. Furthermore, when the  $\text{V}^{5+}$  coverage is beyond 1 ML, multiple  $\text{VO}_x$  layers are predicted to form a layered  $\text{V}_2\text{O}_5$  orthorhombic sheet-like structure,<sup>44</sup> which is expected to be incommensurate with the substrate rutile lattice, as found by the XSW measurements. Cyclohexane molecules react with the V=O bonds, reducing the  $\text{VO}_x$  and forming benzene and  $\text{H}_2\text{O}$ . This reduction not only changes  $\text{V}^{5+}$  to  $\text{V}^{4+}$  but also causes the transformation from an uncorrelated tetrahedral  $\text{VO}_4$  structure to a correlated rutile-like structure. V–O–V and V–O–Ti linkages are created due to the strongly correlated V structure. A detailed atomic interface model is proposed for the Re V structure in Figure 4b, showing the V located on cation lattice sites in the  $\alpha$ - $\text{TiO}_2(110)$  rutile structure and the formation of two- and three-coordinate oxygen atoms.

In summary, we have combined in situ XSW and DRIFTS with ex situ XPS and AFM to comprehensively study the surface transformations that accompany the catalytic dehydrogenation of cyclohexane on ML  $\text{VO}_x$  supported on rutile. The measurements demonstrate that not all of the surface vanadium participates in the oxidation–reduction cycle. The V surface ions change from 100%  $\text{V}^{5+}$  to 61%  $\text{V}^{4+}$ , concurrent with a 100% uncorrelated to 60% correlated structural change, while cyclohexane is oxidized to benzene. Our results show that the V=O is lost in the reduction of the catalyst during the first half-cycle in the ODH reaction. Our structure–property study provides the direct atomic-scale information for molecule–catalyst interactions during ODH. This combined-technique strategy has important implications for understanding a range of catalytic reactions at the atomic scale. In future XSW measurements of such surface reactions, rather than just observing the element-specific XRF signal modulation due to the XSW phase shift, we would measure the chemical-state-specific XPS signal modulation. From this directly combined XSW–XPS measurement, we would produce chemical-state-specific 3D atomic maps. For the above Re case, we could directly determine if, as suspected, the  $\text{V}^{4+}$  were the correlated species and  $\text{V}^{5+}$  the uncorrelated. Future studies of partially Re surfaces would simulate the state of the surface under operando conditions where most of the vanadium is in the 5+ state.

Moreover, knowledge of the structural and chemical state transformations in each separate reaction step, together with operando measurements under real catalytic conditions, would provide a more complete atomic view of the structure–activity relationships.

## EXPERIMENTAL METHODS

**Sample Preparation.** Rutile ( $\alpha$ -TiO<sub>2</sub>) single crystals were oriented, cut ( $10 \times 10 \times 1$  mm<sup>3</sup>), and polished parallel to the (110) by Crystal GmbH (Berlin, Germany) with a miscut < 0.1°. Rutile  $\alpha$ -TiO<sub>2</sub> has a tetragonal crystal structure (space group  $P4_2/mnm$ ) with a room-temperature lattice constant of  $a = b = 4.594$  Å and  $c = 2.959$  Å.  $\alpha$ -TiO<sub>2</sub>(110) substrates were first annealed in a tube furnace with flowing O<sub>2</sub> (~100 sccm) at 400 °C for 0.5 h and then at 1000 °C for 1 h. Prior to ALD, the single-crystal substrates were immersed in ultrapure water (resistivity > 10<sup>18</sup> Ω cm<sup>-1</sup>) for 1 h at 90 °C to hydroxylate the surface. The substrates were then rinsed with 10% HCl, followed by an ultrapure water rinse, and then blown dry with nitrogen. After loading into the ALD reactor,<sup>45</sup> the substrates were stabilized at 100 °C under ultra-high-purity nitrogen at a 300 sccm flow rate and 1 Torr of pressure for 20 min and further cleaned in situ with flowing ozone for 10 min. For the VO<sub>x</sub> ALD, the substrates were exposed first to vanadium oxytriisopropoxide (VOTP, Sigma Aldrich), at a partial pressure of 0.05 Torr for 2 s, followed by a nitrogen purge for 5 s. The substrates were then exposed to hydrogen peroxide at a partial pressure of 0.2 Torr for 2 s, followed by a nitrogen purge for 5 s (2–5–2–5 s). This process is defined as one ALD cycle, or 1c-s, where “s” denotes single crystal. Single-crystal  $\alpha$ -TiO<sub>2</sub>(110) substrates were exposed to two VO<sub>x</sub> ALD cycles to obtain a ML V coverage. After loading the  $\alpha$ -TiO<sub>2</sub> powder (Alfa Aesar) support into the ALD reactor, the sample was stabilized at 100 °C and then given a 10 min ozone cleaning to remove surface carbonyls. The ALD precursor exposure and purge times were increased to 120–120–240–120 s (or 1c-p, where “p” denotes for powder) to account for the larger surface area and increased vapor transport time for the powder relative to those of the coating planar surfaces. These are the AD samples.

The Ox and Re surfaces were prepared by annealing at 400 °C for 30 min in O<sub>2</sub> (~100 sccm) and cyclohexane carried by helium gas (~30 sccm) through a bubbler at 760 Torr, respectively. For ex situ XPS measurements, the reactions were carried out in a quartz tube furnace. After each reaction and cooling down to room temperature with corresponding gas flow, the sample was immediately transferred through the air to the ultrahigh vacuum (UHV) chamber of the XPS system. For in situ XSW, oxidation–reduction reactions were carried out in a beryllium-dome reaction cell. Before any treatment and after each reaction, XSW measurements were carried out at room temperature in the beryllium-dome at a vacuum level held by a diaphragm roughing pump. The pressure was held at ~10<sup>-2</sup> Torr to prevent contamination from outside. During the first oxidation treatment, vanadium was fully oxidized to the 5+ state, and the sample was dehydrated due to removal of adventitious adsorbed water. For in situ DRIFTS measurements, the oxidation was carried out in 10% oxygen in helium at a flow rate of 100 sccm at 400 °C for 20 min. The reduction was performed at 400 °C for 10 min by introducing cyclohexane vapor, which was carried by helium at a flow rate of 50 sccm through a cyclohexane bubbler. The Ox<sub>2</sub> surface was then obtained using the same procedure as that for the Ox surface.

**Characterization.** The surface morphology was studied by AFM with a JEOL-JSPM-5200 scanning probe microscope using silicon AFM tips with a nominal 10 nm radius of curvature and cantilever resonant frequency of 200 kHz. Ex situ XPS was used to examine the surface morphology and chemical states of the surface atoms after each step of the reaction process. The XP spectra were collected with an Omicron ESCA probe using monochromated Al K $\alpha$  X-rays. A low-energy electron flood gun was used to compensate the XPS-induced surface charging effects. Carbon 1s (with binding energy BE = 284.8 eV) was used as the reference to calibrate the XP spectra. For the XSW and XRF analysis, the ALD-processed substrate was placed on a ceramic heating stage inside of a beryllium-dome gas reaction cell that was mounted on a five-circle diffractometer at the Advanced Photon Source (APS) 5ID-C station.<sup>46</sup> The coverage of V on a rutile single crystal was determined to be 1.50 ML by XRF comparison to a calibrated standard sample. The V coverage on powders with three and six cycles of 120–120–240–120 expositions was determined to be 1.25 and 2.50 ML, respectively, by comparing the XPS ratios of V 2p to Ti 2p peak areas for V on single crystals and powders. In situ DRIFTS measurements were performed at room temperature between redox cycles using a Thermo Nicolet Nexus 870 instrument with a mercury–cadmium–telluride detector. The background spectrum was taken on the rutile TiO<sub>2</sub> powder after calcination at 200 °C for 20 min in 10% oxygen in helium and cooling back to room temperature in ultra-high-purity (99.999%) helium at a flow rate of 100 sccm. The ALD 6c-p VO<sub>x</sub>/TiO<sub>2</sub> sample was then loaded into the DRIFTS cell to collect spectra and perform the redox treatments. (The V DRIFTS signal from the 3c-p sample was too weak for detection.) All of the spectra were collected after cooling to room temperature in helium (512 scans, a resolution of 4 cm<sup>-1</sup>).

**Catalytic Performance Tests.** The selectivity and reactivity of VO<sub>x</sub> on cyclohexane ODH were tested on powder samples using the equipment described elsewhere.<sup>8</sup> The reaction was carried out in the temperature range of 325–425 °C; 50 mg of catalyst was diluted with 200 mg of SiC to avoid hot spots during the catalyst testing. Cyclohexane was delivered from a cyclohexane bubbler at room temperature by argon. The flow rates for cyclohexane, oxygen, and argon were 0.22, 0.44, and 19.34 sccm, respectively.

## ASSOCIATED CONTENT

### Supporting Information

Details about AFM, XSW, XRF, and XPS characterization methods, and catalytic performance tests. This material is available free of charge via the Internet at <http://pubs.acs.org>.

## AUTHOR INFORMATION

### Corresponding Author

\*E-mail: [bedzyk@northwestern.edu](mailto:bedzyk@northwestern.edu).

### Notes

The authors declare no competing financial interest.

## ACKNOWLEDGMENTS

This work was supported by the Institute for Catalysis in Energy Processes (U.S. Department of Energy, Office of Basic Energy Sciences, Chemical Sciences Grant DE-FG02-03ER15457). X-ray measurements were performed at the Argonne National Laboratory Advanced Photon Source, Sector

5 (DND-CAT), which is supported by U.S. Department of Energy Grant DE-AC02-06CH11357. DND-CAT is supported by E. I. duPont de Nemours & Co., Northwestern University, and The Dow Chemical Co. J.L. and J.W.E. were supported as part of the DOE, Office of Basic Energy Sciences, Chemical Sciences under the Hydrogen Fuel Initiative program. The AFM, XPS, and DRIFTS measurements used the NIFTI and Keck-II facilities at Northwestern University. This work made use of NU Central Facilities supported by the MRSEC through NSF Contract No. DMR-1121262.

## REFERENCES

- (1) Park, D. H.; Kim, S. S.; Wang, H.; Pinnavaia, T. J.; Papapetrou, M. C.; Lappas, A. A.; Triantafyllidis, K. S. Selective Petroleum Refining Over a Zeolite Catalyst with Small Intracrystal Mesopores. *Angew. Chem., Int. Ed.* **2009**, *48*, 7645–7648.
- (2) Banas, J.; Najbar, M.; Tomasic, V. Kinetic Investigation of the NO Decomposition over V–O–W/Ti(Sn)O<sub>2</sub> Catalyst. *Catal. Today* **2008**, *137*, 267–272.
- (3) Surnev, S.; Ramsey, M. G.; Netzer, F. P. Vanadium Oxide Surface Studies. *Prog. Surf. Sci.* **2003**, *73*, 117–165.
- (4) Kim, C. Y.; Elam, J. W.; Stair, P. C.; Bedzyk, M. J. Redox Driven Crystalline Coherent–Incoherent Transformation for a 2 ML VO<sub>x</sub> Film Grown on  $\alpha$ -TiO<sub>2</sub>(110). *J. Phys. Chem. C* **2010**, *114*, 19723–19726.
- (5) Kim, C. Y.; Escudro, A. A.; Stair, P. C.; Bedzyk, M. J. Atomic-Scale View of Redox-Induced Reversible Changes to a Metal-Oxide Catalytic Surface: VO<sub>x</sub>/( $\alpha$ -Fe<sub>2</sub>O<sub>3</sub>(0001)). *J. Phys. Chem. C* **2007**, *111*, 1874–1877.
- (6) Baron, M.; Abbott, H.; Bondarchuk, O.; Stacchiola, D.; Uhl, A.; Shaikhutdinov, S.; Freund, H. J.; Popa, C.; Ganduglia-Pirovano, M. V.; Sauer, J. Resolving the Atomic Structure of Vanadia Monolayer Catalysts: Monomers, Trimers, and Oligomers on Ceria. *Angew. Chem., Int. Ed.* **2009**, *48*, 8006–8009.
- (7) Shapovalov, V.; Metiu, H. VO<sub>x</sub> ( $x = 1-4$ ) Submonolayers Supported on Rutile TiO<sub>2</sub>(110) and CeO<sub>2</sub>(111) Surfaces: The Structure, The Charge of the Atoms, the XPS Spectrum, and the Equilibrium Composition in the Presence of Oxygen. *J. Phys. Chem. C* **2007**, *111*, 14179–14188.
- (8) Feng, H.; Elam, J. W.; Libera, J. A.; Pellin, M. J.; Stair, P. C. Oxidative Dehydrogenation of Cyclohexane over Alumina-Supported Vanadium Oxide Nanoliths. *J. Catal.* **2010**, *269*, 421–431.
- (9) Stair, P. C.; Marshall, C.; Xiong, G.; Feng, H.; Pellin, M. J.; Elam, J. W.; Curtiss, L.; Iton, L.; Kung, H.; Kung, M. Novel, Uniform Nanostructured Catalytic Membranes. *Top. Catal.* **2006**, *39*, 181–186.
- (10) Kilos, B.; Bell, A. T.; Iglesia, E. Mechanism and Site Requirements for Ethanol Oxidation on Vanadium Oxide Domains. *J. Phys. Chem. C* **2009**, *113*, 2830–2836.
- (11) Tian, H. J.; Ross, E. I.; Wachs, I. E. Quantitative Determination of the Speciation of Surface Vanadium Oxides and Their Catalytic Activity. *J. Phys. Chem. B* **2006**, *110*, 9593–9600.
- (12) Weckhuysen, B. M.; Keller, D. E. Chemistry, Spectroscopy and the Role of Supported Vanadium Oxides in Heterogeneous Catalysis. *Catal. Today* **2003**, *78*, 25–46.
- (13) Feng, Z.; Cheng, L.; Kim, C.-Y.; Elam, J. W.; Zhang, Z.; Curtiss, L. A.; Zapol, P.; Bedzyk, M. J. Atomic-Scale Study of Ambient-Pressure Redox-Induced Changes for an Oxide-Supported Submonolayer Catalyst: VO<sub>x</sub>/( $\alpha$ -TiO<sub>2</sub>(110)). *J. Phys. Chem. Lett.* **2012**, *3*, 2845–2850.
- (14) Agnoli, S.; Sambti, M.; Granozzi, G.; Castellarin-Cudia, C.; Surnev, S.; Ramsey, M. G.; Netzer, F. P. The Growth of Ultrathin Films of Vanadium Oxide on TiO<sub>2</sub>(110). *Surf. Sci.* **2004**, *562*, 150–156.
- (15) Goodman, D. W. Model Studies in Catalysis Using Surface Science Probes. *Chem. Rev.* **1995**, *95*, 523–536.
- (16) More hydroxyl (OH) groups on the Ox surface as compared to the Re surface is most likely due to water adsorption on the surface during the sample transfer process from the reaction furnace to XPS chamber. This water is removed during the formation of the Re surface.
- (17) Kim, C. Y.; Klug, J. A.; Stair, P. C.; Bedzyk, M. J. Hydration and Reduction of Molecular Beam Epitaxy Grown VO<sub>x</sub>/( $\alpha$ -Fe<sub>2</sub>O<sub>3</sub>(0001)): Ambient Pressure Study. *J. Phys. Chem. C* **2009**, *113*, 1406–1410.
- (18) Silversmit, G.; Depla, D.; Poelman, H.; Marin, G. B.; De Gryse, R. Determination of the V2p XPS Binding Energies for Different Vanadium Oxidation States (V<sup>5+</sup> to V<sup>0+</sup>). *J. Electron Spectrosc.* **2004**, *135*, 167–175.
- (19) Shah, P. R.; Vohs, J. M.; Gorte, R. J. Redox Isotherms for Vanadia Supported on Zirconia. *Catal. Lett.* **2008**, *125*, 1–7.
- (20) Koranne, M. M.; Goodwin, J. G.; Marcelin, G. Characterization of Silica-Supported and Alumina-Supported Vanadia Catalysts Using Temperature-Programmed Reduction. *J. Catal.* **1994**, *148*, 369–377.
- (21) Bedzyk, M. J.; Cheng, L. X-ray Standing Wave Studies of Minerals and Mineral Surfaces: Principles and Applications. *Rev. Mineral. Geochem.* **2002**, *49*, 221–266.
- (22) Zeegenhagen, J. Surface-Structure Determination with X-Ray Standing Waves. *Surf. Sci. Rep.* **1993**, *18*, 199–271.
- (23) Woodruff, D. P. Surface Structure Determination Using X-ray Standing Waves. *Rep. Prog. Phys.* **2005**, *68*, 743–798.
- (24) Cheng, L.; Fenter, P.; Bedzyk, M. J.; Sturchio, N. C. Fourier-Expansion Solution of Atom Distributions in a Crystal Using X-ray Standing Waves. *Phys. Rev. Lett.* **2003**, *90*, 255503.
- (25) Zhang, Z.; Fenter, P.; Cheng, L.; Sturchio, N. C.; Bedzyk, M. J.; Machesky, M. L.; Wesolowski, D. J. Model-Independent X-ray Imaging of Adsorbed Cations at the Crystal–Water Interface. *Surf. Sci.* **2004**, *554*, L95–L100.
- (26) Okasinski, J. S.; Kim, C.; Walko, D. A.; Bedzyk, M. J. X-ray Standing Wave Imaging of the 1/3 Monolayer Sn/Ge-(111) Surface. *Phys. Rev. B* **2004**, *69*, 041401.
- (27) Feng, Z.; Kim, C.-Y.; Elam, J. W.; Ma, Q.; Zhang, Z.; Bedzyk, M. Direct Atomic-Scale Observation of Redox-Induced Cation Dynamics in an Oxide-Supported Monolayer Catalyst: WO<sub>x</sub>/( $\alpha$ -Fe<sub>2</sub>O<sub>3</sub>(0001)). *J. Am. Chem. Soc.* **2009**, *131*, 18200.
- (28) Because the V K $\alpha$  (4.95 keV) peak was buried under the strong Ti K $\beta$  (4.93 keV) peak, the V K $\beta$  (5.43 keV) peak, which is separable from the tail of the Ti K $\beta$  peak (Figure S2, SI), was used for the XSW analysis. See Figure S2 (SI) for more details.
- (29) Kim, C. Y.; Elam, J. W.; Pellin, M. J.; Goswami, D. K.; Christensen, S. T.; Hersam, M. C.; Stair, P. C.; Bedzyk, M. J. Imaging of Atomic Layer Deposited (ALD) Tungsten Monolayers on  $\alpha$ -TiO<sub>2</sub>(110) by X-ray Standing Wave Fourier Inversion. *J. Phys. Chem. B* **2006**, *110*, 12616–12620.
- (30) Diebold, U. The Surface Science of Titanium Dioxide. *Surf. Sci. Rep.* **2003**, *48*, 53–229.
- (31) Della Negra, M.; Sambti, M.; Granozzi, C. The Structure of an Ultrathin VO<sub>x</sub> ( $x$  approximate to 1) Film Grown Epitaxially on TiO<sub>2</sub>(110) (vol 461, pg 118, 2000). *Surf. Sci.* **2001**, *461*, 118.
- (32) Kroger, E. A.; Allegretti, F.; Knight, M. J.; Polcik, M.; Sayago, D. I.; Woodruff, D. P.; Dhanak, V. R. Structural Characterisation of Ultrathin VO<sub>x</sub> Films on TiO<sub>2</sub>(110). *Surf. Sci.* **2006**, *600*, 4813–4824.
- (33) Sambti, M.; Sangiovanni, G.; Granozzi, G.; Parmigiani, F. Growth and the Structure of Epitaxial VO<sub>2</sub> at the TiO<sub>2</sub>(110) Surface. *Phys. Rev. B* **1997**, *55*, 7850–7858.
- (34) Bulushev, D. A.; Reshetnikov, S. I.; Kiwi-Minsker, L.; Renken, A. Deactivation Kinetics of V/Ti-Oxide in Toluene Partial Oxidation. *Appl. Catal., A* **2001**, *220*, 31–39.
- (35) Ramis, G.; Busca, G.; Bregani, F. On the Effect of Dopants and Additives on the State of Surface Vanadyl Centers of Vanadia–Titania Catalysts. *Catal. Lett.* **1993**, *18*, 299–303.
- (36) Scharf, U.; Schneider, M.; Baiker, A.; Wokaun, A. Vanadia–Titania Aerogels. 2. Spectroscopic Investigation of the Structural Properties. *J. Catal.* **1994**, *149*, 344–355.
- (37) Borovkov, V. Y.; Mikheeva, E. P.; Zhidomirov, G. M.; Lapina, O. B. Theoretical and Experimental Studies of the Nature of the Catalytic Activity of VO<sub>x</sub>/TiO<sub>2</sub> Systems. *Kinet. Catal.* **2003**, *44*, 710–717.

(38) Wegener, S. L.; Kim, H.; Marks, T. J.; Stair, P. C. Precursor Nuclearity Effects in Supported Vanadium Oxides Prepared by Organometallic Grafting. *J. Phys. Chem. Lett.* **2011**, *2*, 170–175.

(39) Kim, H.; Kosuda, K. M.; Van Duyne, R. P.; Stair, P. C. Resonance Raman and Surface- And Tip-Enhanced Raman Spectroscopy Methods to Study Solid Catalysts and Heterogeneous Catalytic Reactions. *Chem. Soc. Rev.* **2010**, *39*, 4820–4844.

(40) Gao, X. T.; Bare, S. R.; Fierro, J. L. G.; Wachs, I. E. Structural Characteristics and Reactivity/Reducibility Properties of Dispersed and Bilayered  $V_2O_5/TiO_2/SiO_2$  Catalysts. *J. Phys. Chem. B* **1999**, *103*, 618–629.

(41) Banares, M. A.; Wachs, I. E. Molecular Structures of Supported Metal Oxide Catalysts under Different Environments. *J. Raman Spectrosc.* **2002**, *33*, 359–380.

(42) Khodakov, A.; Olthof, B.; Bell, A. T.; Iglesia, E. Structure and Catalytic Properties of Supported Vanadium Oxides: Support Effects on Oxidative Dehydrogenation Reactions. *J. Catal.* **1999**, *181*, 205–216.

(43) Goebke, D.; Romanyshyn, Y.; Guimond, S.; Sturm, J. M.; Kuhlbeck, H.; Dobler, J.; Reinhardt, U.; Ganduglia-Pirovano, M. V.; Sauer, J.; Freund, H. J. Formaldehyde Formation on Vanadium Oxide Surfaces  $V_2O_3(0001)$  and  $V_2O_5(001)$ : How Does the Stable Methoxy Intermediate Form? *Angew. Chem., Int. Ed.* **2009**, *48*, 3695–3698.

(44) Blum, R. P.; Niehus, H.; Hucho, C.; Fortrie, R.; Ganduglia-Pirovano, M. V.; Sauer, J.; Shaikhutdinov, S.; Freund, H. J. Surface Metal-Insulator Transition on A Vanadium Pentoxide (001) Single Crystal. *Phys. Rev. Lett.* **2007**, *99*, 226103.

(45) Elam, J. W.; Groner, M. D.; George, S. M. Viscous Flow Reactor with Quartz Crystal Microbalance for Thin Film Growth by Atomic Layer Deposition. *Rev. Sci. Instrum.* **2002**, *73*, 2981–2987.

(46) Walko, D. A.; Sakata, O.; Lyman, P. F.; Lee, T.-L.; Tinkham, B. P.; Okasinski, J. S.; Zhang, Z.; Bedzyk, M. J. Surface and Interface Studies at APS Endstation SID-C. In *Synchrotron Radiation Instrumentation: Eighth International Conference*; Warwick, T., Arthur, J., Padmore, H. A., Stohr, J., Eds.; American Institute of Physics: New York, 2004; pp 1166–1169.